RSC Sustainability

ROYAL SOCIETY OF CHEMISTRY

PAPER

View Article Online
View Journal | View Issue

Cite this: *RSC Sustainability*, 2024, **2**, 1128

In silico exploration of acetic acid driven multicomponent synthesis: design, characterization, and antioxidant evaluation of spiroacridines and spiroquinolines†

Subham G. Patel,[ab] Dipti B. Upadhyay,[a] Nirajkumar V. Shah,[b] Mehul P. Parmar,[a] Paras J. Patel,[a] Apoorva Malik,[c] Rakesh K. Sharma[c] and Hitendra M. Patel*[a]

In this study, a highly efficient green synthetic protocol was developed for the synthesis of spiroacridines and spiroquinolines *via* a multicomponent reaction of 3,4-methylenedioxyaniline, isatin and cyclic 1,3-diones in glacial acetic acid. This metal-free multicomponent approach offers mild reaction conditions, shorter reaction time and easy product purification without column chromatography. Frontier molecular orbitals (FMOs), various quantum chemical descriptors (QCDs) and molecular electrostatic potential (MEP) surfaces were computed using density functional theory (DFT) with a B3LYP/6-311G+(d,p) basis set. All newly synthesized compounds were screened for their antioxidant properties. The compounds **4a** and **4v** are the most potent ABTS and DPPH radical scavengers to the standard ascorbic acid. *In silico* molecular docking studies were conducted to determine the binding affinities of the most potent **4a** and **4v** with targeted antioxidant protein, LD-carboxypeptidase, which show a strong binding affinity of −10.5 kcal mol^{-1} and −10.7 kcal mol^{-1}, respectively. The most potent antioxidants **4a** and **4v** were evaluated for *in silico* drug-likeness and ADME prediction.

Received 18th January 2024
Accepted 10th March 2024

DOI: 10.1039/d4su00024b

rsc.li/rscsus

Sustainability spotlight

We synthesized a novel spiroacridines and spiroquinolines using one pot multicomponent reactions of 3,4-methylenedioxyaniline, isatin and cyclic 1,3-diones in presence of glacial acetic acid. This reactions protocol covers broad sustainable approaches such as metal-free, mild reaction conditions, shorter reaction time and easy product purification without using column chromatography. The claimed derivatives provides a promising antioxidants property and drug likeness properties.

1. Introduction

Reactive oxygen species (ROS) play an integral role in the development of many major illnesses, including cancer, diabetes, arteriosclerosis, heart disease, and cataracts.[1] The detrimental effects of free radicals that may cause biological damage are referred to as oxidative stress. Free radicals have a pathogenic role in the development of a wide range of chronic degenerative illnesses in humans, including cancer and autoimmune, inflammatory, and cardiovascular neurodegenerative disorders.[2,3] Free radicals are chemical entities that possess an unpaired electron. By grasping an electron from a neighbouring biomolecule, these free radicals initiate a chain reaction in the human body, causing them to behave abnormally in living systems. Antioxidants are compounds that donate electrons to free radicals in order to transform them into non-harmful substances. In a nutshell, antioxidants protect the body from oxidative stress by suppressing the oxidation process.[4] As a result, the necessity to produce antioxidant drugs has grown in recent years.

In present times, the use of sustainable synthetic protocols has received much more attention for the construction of novel heterocycles.[5] For the construction of various heterocycles of biological interest, multicomponent reactions are most commonly used to form multiple C–C and C–N bonds without the isolation of an intermediate. MCRs are more vulnerable than classical multistep synthesis owing to their higher reaction efficiency and straightforward operation.[6,7] New spiroacridines and spiroquinolines were made using this multicomponent synthetic approach. It has encouraged the synthetic community to seek out more environmentally friendly syntheses and

[a]*Department of Chemistry, Sardar Patel University, Vallabh Vidyanagar-388120, Gujarat, India. E-mail: hm_patel@spuvvn.edu*

[b]*J & J College of Science, Nadiad-387001, Kheda, Gujarat, India*

[c]*Sustainable Materials and Catalysts Research Laboratory (SMCRL), Department of Chemistry, Indian Institute of Technology, Jodhpur, India*

† Electronic supplementary information (ESI) available. See DOI: https://doi.org/10.1039/d4su00024b

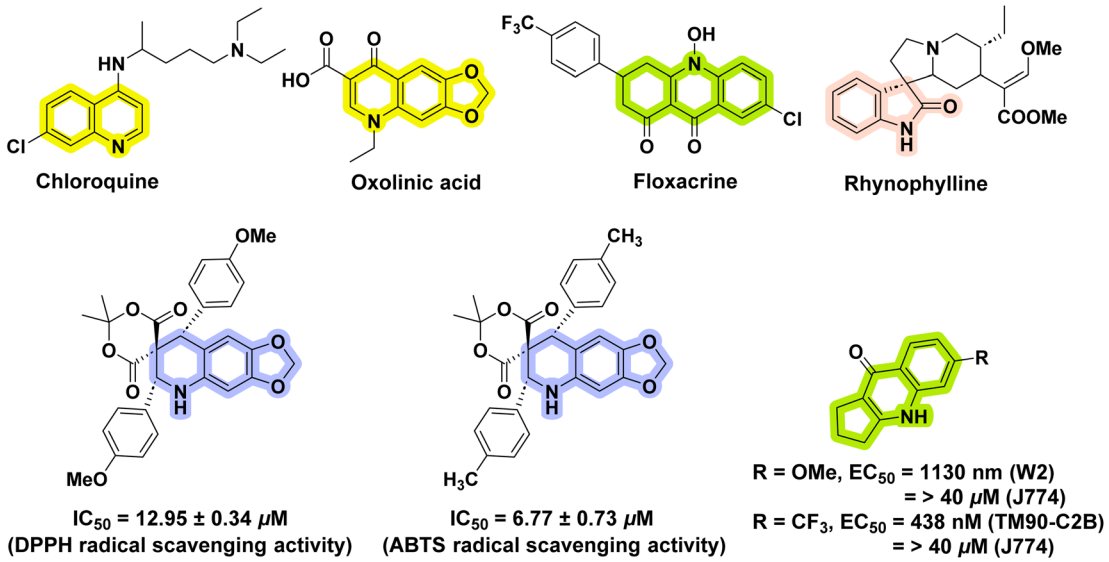

Fig. 1 Acridine, quinoline, 1,3-benzodioxole and spiroindoline-based biologically active compounds.

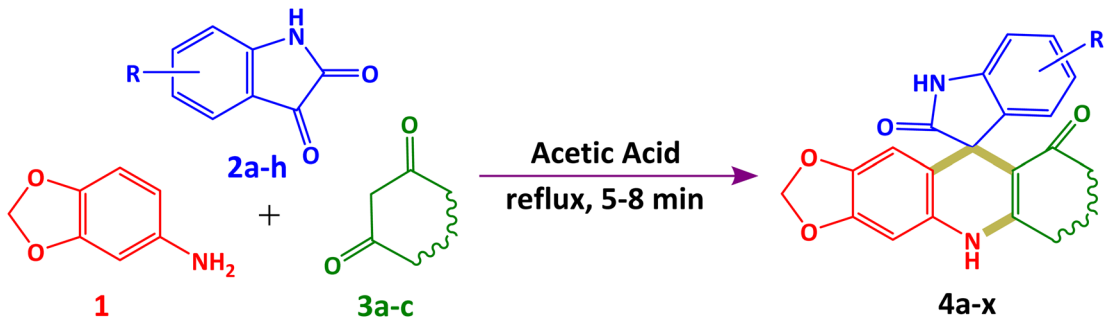

Scheme 1 Multicomponent synthesis of **4a** from 3,4-methylenedioxyaniline **1**, isatins **2a–h**, and cyclic 1,3-diones **3a–c**.

reactions in order to speed up preparation while using less energy and effort.[1,8]

Nitrogen-containing heterocycles are significant in medicinal chemistry and drug design, as evidenced by their preponderance in marketed drugs.[9] Spiroindolines have grabbed the interest of researchers due to their privileged structural moiety and occurrence in a wide range of bioactive natural products and synthesised drugs.[10] Acridines and quinolines are interesting moieties in heterocyclic chemistry that attract the most attention to chemical modifications and are promising chemical entities both synthetically and medicinally due to their diverse pharmacological applications such as anticancer,[11,12] SRC kinase inhibitory,[13,14] antioxidant,[15,16] and antiallergic activity.[17] Fig. 1 depicts several acridine,[18] quinoline,[19,20] spiroindoline[21] and 1,3-benzodioxole[22] conjugates with promising biological applications. The antioxidant activity of the spiroacridine and spiroquinoline moieties has received little attention. We were inspired to create acridine and quinoline-containing spiroacridines and spiroquinolines as a result of this.

In continuation to our efforts towards the construction of novel spiro molecules,[16,23–26] herein, we explored a metal-free multicomponent synthesis[1,27–29] of spiroacridines and spiroquinolines *via* a one-pot reaction of 3,4-methylenedioxyaniline, isatin and cyclic 1,3-diones in the presence of glacial acetic acid, which is vital for sustainability (Scheme 1). To acquire theoretical insights, the frontier molecular orbital (FMO), the molecular electrostatic potential (MEP), and several quantum chemical descriptors (QCDs) were computed using the DFT using the B3LYP/6-311G+(d,p) basis set. All the newly synthesised spiro molecules were screened for their antioxidant properties.

2. Results and discussion

2.1. Chemistry

In this protocol, we selected 3,4-methylenedioxyaniline **1** (1 mmol), isatin **2a** (1 mmol), and dimedone **3a** (1 mmol) as a model reaction in order to achieve our target spiro heterocyclic moiety 7′,7′-dimethyl-7′,8′-dihydro-5′*H*-spiro[indoline-3,10′-[1,3]dioxolo[4,5-*b*]acridine]-2,9′(6′*H*)-dione **4a** under catalyst-free conditions *via* multicomponent synthesis. In order to check the effect of temperature and solvents, we optimized our model reaction by using a variety of solvents at different temperatures. In the initial phase, we initiated our model

Table 1 Optimization of reaction for the preparation of compound **4a** [a]

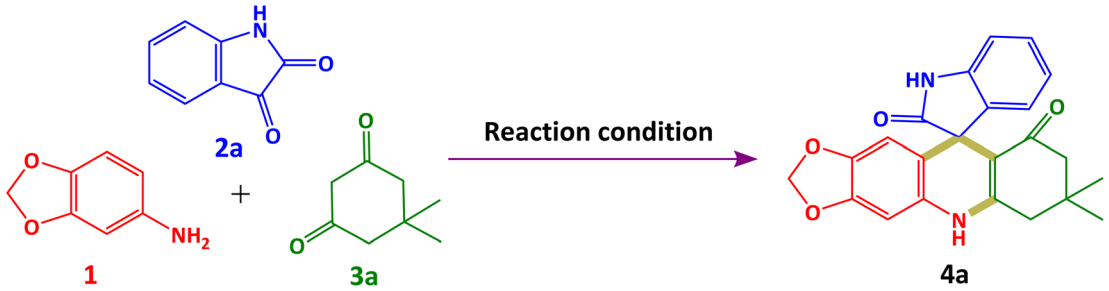

Entry	Solvent[b]	Temperature	Time	Conversion relative to isatin[c]
1	Water	rt	6 h	NR
2	Ethanol	rt	6 h	NR
3	Ethanol	Reflux	45 min	100%
4	Methanol	Reflux	45 min	100%
5	Ethyl L-lactate	Reflux	90 min	100%
6	**Acetic acid**	**Reflux**	**5 min**	**100%**
7	DMF	Reflux	4 h	Incomplete
8	Acetonitrile	Reflux	60 min	100%

[a] Reaction conditions: 1 mmol 3,4-methylenedioxyaniline **1**, 1 mmol isatin **2a** and 1 mmol dimedone **3a**, reflux. [b] 3 mL solvent. [c] Observed from TLC analysis.

reaction employing environmentally friendly solvents, water and ethanol, under room temperature conditions (Table 1, entries 1 and 2). However, no discernible transformation of isatin **2a** into our target compound **4a** was observed. In pursuit of our desired molecule **4a**, we executed our model reaction by elevating the temperature from room temperature to reflux. Subsequently, our model reaction was conducted utilizing ethanol at its reflux temperature (Table 1, entry 3). During this experiment, we noted the production occurring within the reaction medium at its reflux temperature. Thin-layer chromatography analysis indicated a full transformation of **2a** into **4a**, accompanied by the emergence of a novel fluorescence spot on the TLC plate. After that, we performed our model reaction using different organic solvents such as methanol, ethyl L-lactate, acetic acid, DMF and acetonitrile (Table 1, entries 4–8). The best outcomes were achieved when glacial acetic acid was used (Table 1, entry 6). In the presence of glacial acetic acid, we observed rapid transformation of **2a** into **4a** within just 5 minutes under reflux conditions. Therefore, we selected it as the best optimum condition for the synthesis of our target moiety 7′,7′-dimethyl-7′,8′-dihydro-5′*H*-spiro[indoline-3,10′-[1,3]dioxolo[4,5-*b*]acridine]-2,9′(6′*H*)-dione **4a**. It is noteworthy that acetic acid is the sole solvent containing acidic hydrogen among all solvents, playing a dual role as both the catalyst and solvent. This dual functionality enhances reaction efficiency and reduces overall reaction time.

Using this best optimum condition, we systematically explored the substrate scope for synthesizing spiroacridines **4a–p** and spiroquinolines **4q–x**. This exploration involved utilizing 3,4-methylenedioxyaniline **1** (1 mmol), various substituted isatins **2a–h** (1 mmol), and diverse cyclic 1,3-diones **3a–c** (1 mmol) in the presence of glacial acetic acid at reflux temperature. In the presence of various substituted isatins **2a–h** and various cyclic 1,3-diones, all reactions proceeded smoothly and furnished final moieties **4a–x** with good isolated yield ranging from 68–78% within the stipulated time range. The results are summarized in Table 2. Fortunately, we discovered the solidification of the final product following the reaction transformation in each set of studies. The primary investigation for the confirmation of the desired product is carried out by the thin layer chromatography method using 70% ethyl acetate and 30% *n*-hexane as the mobile phase. The structures of all newly synthesized compounds are characterized by ^{1}H NMR, ^{13}C NMR and HRMS spectral analysis.

2.2. Density functional theory calculations

2.2.1. Frontier molecular orbital (FMO) analysis. In this study, we analysed frontier molecular orbitals (FMOs) to gain insights into stability, reactive properties, molecular interactions and physicochemical properties of newly synthesised spiroacridines **4a–p** and spiroquinolines **4q–x** by using density functional theory (DFT) calculations. The lowest unoccupied molecular orbital (LUMO) and the highest occupied molecular orbital (HOMO) are the two primary molecular orbitals associated with reactions with other molecular structures, respectively. The DFT/B3LYP method with a 6-311G+(d,p) basis set was used to calculate the energies of HOMO and LUMO and their orbital energy gap E_{gap} of spiro compounds **4a–x**. The HOMO–LUMO graphical depiction of molecules **4a**, **4i** and **4q** is shown in Fig. 2. Positive and negative areas are represented by red and green colours, respectively. Compounds **4a**, **4i** and **4q** contain a dimedone, cyclohexane 1,3-dione and cyclopentane 1,3-dione ring moiety, respectively. A lower orbital energy gap denotes

Table 2 Substrate scope of the synthesis of spiroacridines **4a–p** and spiroquinolines **4q–x** [a]

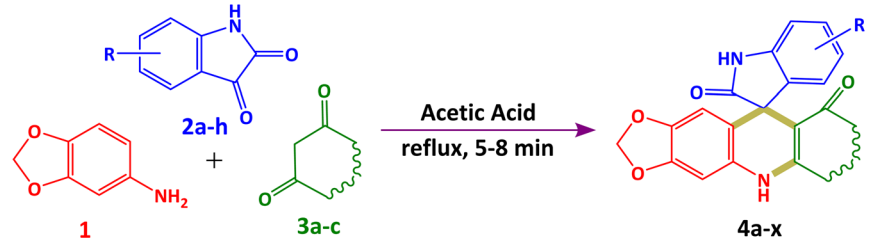

4a 74%, 5 min	**4b** 72%, 6 min	**4c** 71%, 6 min	**4d** 75%, 5 min
4e 70%, 7 min	**4f** 78%, 5 min	**4g** 69%, 8 min	**4h** 75%, 6 min
4i 73%, 6 min	**4j** 71%, 7 min	**4k** 70%, 7 min	**4l** 73%, 6 min
4m 69%, 7 min	**4n** 76%, 6 min	**4o** 69%, 8 min	**4p** 73%, 7 min
4q 71%, 7 min	**4r** 70%, 7 min	**4s** 69%, 8 min	**4t** 72%, 6 min
4u 70%, 8 min	**4v** 71%, 7 min	**4w** 68%, 8 min	**4x** 69%, 8 min

[a] Reaction conditions: 1 mmol 3,4-methylenedioxyaniline **1**, 1 mmol isatins **2a–h** and 1 mmol cyclic 1,3-diones **3a–c**, 3 mL glacial acetic acid, reflux.

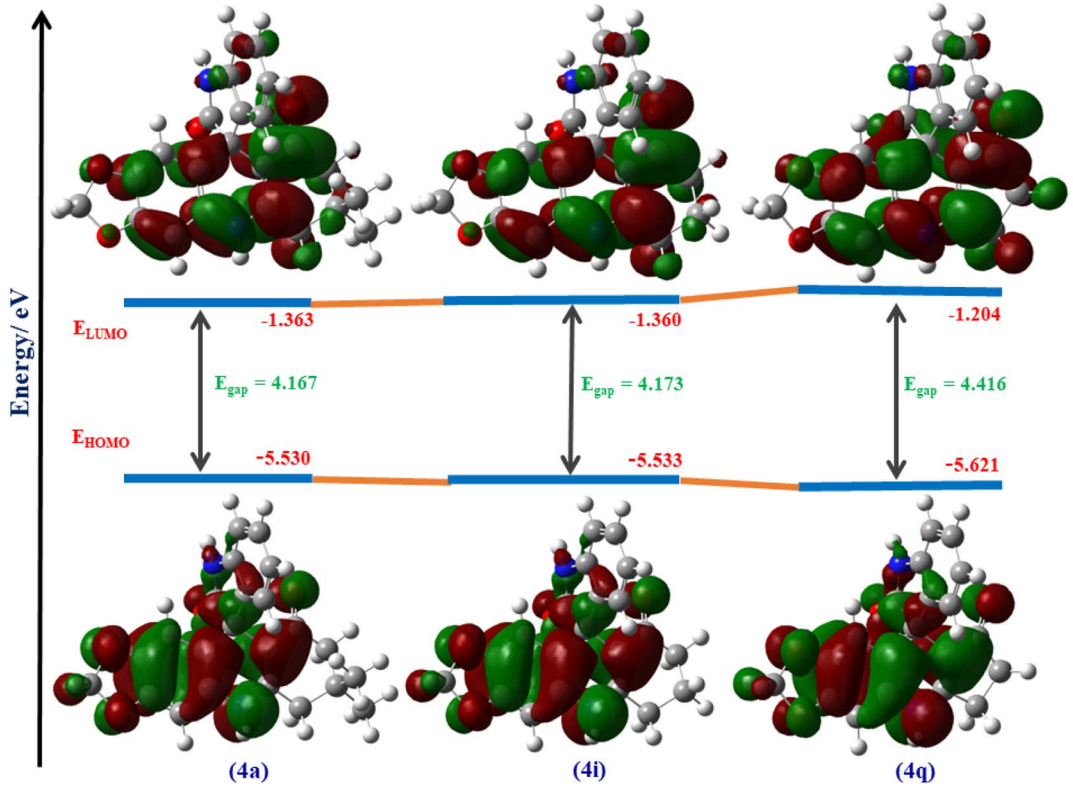

Fig. 2 The HOMO–LUMO energy diagram of molecules **4a**, **4i** and **4j** calculated at DFT/B3LYP/6-311G+(d,p) in the gaseous phase.

more reactivity and less stability. As can be seen from Fig. 2, **4a** with a dimedone ring moiety has higher reactivity and less stability than **4i** and **4q**, whereas **4q** with a cyclopentane 1,3-dione ring moiety has the highest stability and less reactivity.

HOMO and LUMO energies are also used to illustrate various quantum chemical descriptors (QCDs) such as ionisation potential (IP), electron affinity (EA), chemical hardness (η) and softness (σ), electronegativity (χ), chemical potential (μ), electrophilicity index (ω), nucleophilicity index (ε_γ) and maximum charge transfer index (ΔN_{max}). These QCDs were computed using the B3LYP/6-311G+(d,p) basis set, according to Koopman's theorem.[30] These QCDs play an essential role in emphasising the chemical behaviour and reactivity of the target molecule. The computed QCDs of spiro molecules **4a–x** are listed in Table 3.

2.2.2. Molecular electrostatic potential analysis. A mapping of electrostatic potential onto a surface with a constant electron density is called the molecular electrostatic potential, or MEP. The molecular electrostatic potential (MEP) surface is often used to forecast the locations or sections of a molecule that would initially attract an approaching electrophile or nucleophile. The MEP surface of all spiro molecules **4a–x** was calculated using the DFT/B3LYP/6-311G+(d,p) basis set in the gaseous phase. The MEP surface plots of **4a**, **4i** and **4q** are shown in Fig. 3. Different MEP surface values are represented by the different colours in the plots. Here, the dark blue colour indicates the strongest attraction and is most susceptible to nucleophilic attack whereas the dark red colour indicates the strongest repulsion and is most susceptible to electrophilic attack. The majority of the negative areas lie above the O atom of oxygen of both carbonyl groups while the positive area lies above the N atom of nitrogen. According to this settlement, the O atom in this area participates in intermolecular interactions as an acceptor and the N atom in this area participates in intramolecular interactions as a donor in molecules **4a–x**.

2.3. *In vitro* antioxident activity

To identify antioxidant properties of all newly synthesized spiroacridines **4a–p** and spiroquinolines **4q–x**, *in vitro* 2,2′-azinobis(3-ethylbenzothiazoline-6-sulfonic acid) (ABTS) and 2,2-diphenyl-1-picrylhydrazyl (DPPH) radical scavenging activity was tested. As a standard, antioxidant ascorbic acid was used. For ABTS and DPPH radical scavenging assay, it exhibits 41.84 ± 0.25 μM and 90.10 ± 0.70 μM IC_{50} values, respectively. Table 4 displays the antioxidant activities of **4a–x**. All spiro compounds show good radical scavenging activity. Among them **4a** (ABTS, IC_{50} = 22.52 ± 0.82 μM; DPPH, IC_{50} = 19.07 ± 0.23 μM) and **4v** (ABTS, IC_{50} = 21.27 ± 0.58 μM; DPPH, IC_{50} = 59.15 ± 0.29 μM) are the most potent radical scavengers against both ABTS & DPPH radicals which display excellent scavenging activity to standard ascorbic acid (Fig. 4). Meanwhile, all spiro compounds **4a–x** are good ABTS radical scavengers. Spiroacridines **4b** (ABTS, IC_{50} = 36.27 ± 0.74 μM), **4h** (ABTS, IC_{50} = 34.18 ± 0.88 μM), **4i** (ABTS, IC_{50} = 23.75 ± 0.83 μM), **4n** (ABTS, IC_{50} = 24.58 ± 0.76 μM), and **4p** (ABTS, IC_{50} = 22.80 ± 0.74 μM) and spiroquinolines **4r** (ABTS, IC_{50} = 35.85 ± 0.34 μM), **4u** (ABTS, IC_{50} = 23.19

Table 3 Calculated quantum chemical descriptors of spiro molecules **4a–x** [a]

Molecule	E_{HOMO} (eV)	E_{LUMO} (eV)	E_g (eV)	IP (eV)	EA (eV)	η (eV)	σ (eV)	χ (eV)	μ (eV)	ω (eV)	ε_γ (eV)	N (eV)
4a	−5.530	−1.363	4.167	5.530	1.363	2.083	0.240	3.447	−3.447	2.851	−7.181	1.654
4b	−5.645	−1.487	4.158	5.645	1.487	2.079	0.240	3.566	−3.566	3.058	−7.413	1.715
4c	−5.649	−1.484	4.165	5.649	1.484	2.082	0.240	3.567	−3.567	3.054	−7.427	1.713
4d	−5.506	−1.340	4.166	5.506	1.340	2.083	0.240	3.423	−3.423	2.812	−7.129	1.643
4e	−5.641	−1.473	4.168	5.641	1.473	2.084	0.240	3.557	−3.557	3.036	−7.413	1.707
4f	−5.429	−1.285	4.144	5.429	1.285	2.072	0.241	3.357	−3.357	2.719	−6.956	1.620
4g	−5.831	−2.547	3.284	5.831	2.547	1.642	0.305	4.189	−4.189	5.343	−6.878	2.551
4h	−5.627	−1.460	4.167	5.627	1.460	2.084	0.240	3.544	−3.544	3.013	−7.384	1.701
4i	−5.533	−1.360	4.173	5.533	1.360	2.086	0.240	3.446	−3.446	2.847	−7.191	1.652
4j	−5.651	−1.480	4.171	5.651	1.480	2.085	0.240	3.565	−3.565	3.047	−7.435	1.710
4k	−5.656	−1.485	4.170	5.656	1.485	2.085	0.240	3.571	−3.571	3.057	−7.446	1.712
4l	−5.509	−1.336	4.173	5.509	1.336	2.086	0.240	3.422	−3.422	2.807	−7.140	1.640
4m	−5.646	−1.472	4.174	5.646	1.472	2.087	0.240	3.559	−3.559	3.035	−7.428	1.706
4n	−5.462	−1.309	4.152	5.462	1.309	2.076	0.241	3.385	−3.385	2.760	−7.029	1.631
4o	−5.842	−2.543	3.299	5.842	2.543	1.649	0.303	4.192	−4.192	5.328	−6.915	2.542
4p	−5.634	−1.460	4.173	5.634	1.460	2.087	0.240	3.547	−3.547	3.014	−7.401	1.700
4q	−5.621	−1.204	4.416	5.621	1.204	2.208	0.226	3.413	−3.413	2.637	−7.536	1.545
4r	−5.736	−1.322	4.413	5.736	1.322	2.207	0.227	3.529	−3.529	2.822	−7.787	1.599
4s	−5.701	−1.306	4.394	5.701	1.306	2.197	0.228	3.504	−3.504	2.793	−7.698	1.595
4t	−5.596	−1.181	4.415	5.596	1.181	2.208	0.226	3.388	−3.388	2.600	−7.480	1.535
4u	−5.732	−1.153	4.579	5.732	1.153	2.289	0.218	3.442	−3.442	2.588	−7.881	1.504
4v	−5.568	−1.153	4.415	5.568	1.153	2.207	0.227	3.360	−3.360	2.558	−7.418	1.522
4w	−5.920	−2.614	3.306	5.920	2.614	1.653	0.302	4.267	−4.267	5.508	−7.053	2.582
4x	−5.720	−1.306	4.415	5.720	1.306	2.207	0.227	3.513	−3.513	2.795	−7.755	1.591

[a] DFT/B3LYP/6-311G+(d,p) was used in a gaseous state.

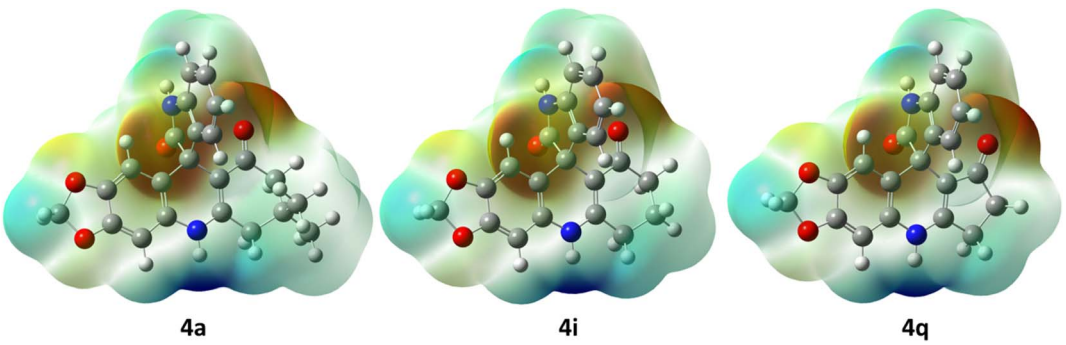

Fig. 3 Molecular electrostatic surface diagram of molecules **4a**, **4i** and **4j** calculated at DFT/B3LYP/6-311G+(d,p) in the gaseous phase.

± 0.23 μM), and **4x** (ABTS, IC_{50} = 27.30 ± 0.26 μM) show excellent ABTS radical scavenging activity.

2.4. *In silico* docking study

Following the observation of outstanding antioxidant activity exhibited by the potent spiroacridine **4a** and spiroquinoline **4v**, a subsequent docking study was conducted. Gram-positive *Listeria monocytogenes* is a widespread intracellular pathogen which is responsible for numerous outbreaks of foodborne illness.[31] So, for the docking study, we have chosen the *Listeria monocytogenes* targeted antioxidant protein in the LD-carboxypeptidase domain. According to the docking analysis, **4a** and **4v** exhibit proficient binding to the receptor's active sites, specifically site-1 and site-3, with respective binding affinities of −10.5 kcal mol^{-1} and −10.7 kcal mol^{-1}, which are subsequently better than −5.4 kcal mol^{-1}, exhibited by the standard drug (ascorbic acid) employed in the antioxidant activity investigation (Fig. 5). Among the receptor's two active sites, **4a** interacts with the active site-1 *via* conventional H-bonds, π-cation type of interaction, carbon–hydrogen bonds, π–π T-shapes, and unfavorable donor–donor type of interaction. The H-atom attached to the indole ring of spiroacridine **4a** shows unfavorable donor–donor type interaction with TYR A:174 (1.94 Å). The carbonyl oxygen of the indole ring and an oxygen atom of 1,3-benzodioxole show conventional H-bonding with ARG A:19 (2.33 Å) and GLY A:85 (2.92 Å), respectively. An aryl ring of 1,3-benzodioxol of **4a** interacts with ARG A:19 (3.65 Å) and HIS A:296 (5.28 Å) through π-cation and π–π T-shaped types of interactions, respectively. Furthermore, the methylene group of 1,3-bonzodioxol of **4a** interacts with GLY A:85 (3.01 Å) through a carbon–hydrogen bond.

Table 4 *In vitro* ABTS and DPPH radical scavenging activities of spiroacridines **4a–x** and spiroquinolines **4q–x**

	ABTS radical scavenging activity	DPPH radical scavenging activity
Compound name	$IC_{50} \pm SEM^a$ (μM)	$IC_{50} \pm SEM^a$ (μM)
4a	**22.52 ± 0.82**	**19.07 ± 0.23**
4b	**36.27 ± 0.74**	156.64 ± 0.49
4c	66.48 ± 0.19	768.70 ± 0.27
4d	66.92 ± 0.53	686.08 ± 0.72
4e	56.39 ± 0.42	695.75 ± 0.64
4f	76.40 ± 0.31	253.01 ± 0.52
4g	48.12 ± 0.36	318.36 ± 0.37
4h	**34.18 ± 0.88**	179.63 ± 0.48
4i	**23.75 ± 0.83**	245.18 ± 0.23
4j	57.70 ± 0.19	897.43 ± 0.18
4k	46.31 ± 0.26	427.61 ± 0.28
4l	48.81 ± 0.38	364.29 ± 0.45
4m	48.97 ± 0.85	942.74 ± 0.34
4n	**24.58 ± 0.76**	262.80 ± 0.72
4o	42.89 ± 0.38	503.96 ± 0.16
4p	**22.80 ± 0.74**	901.44 ± 0.83
4q	42.75 ± 0.59	526.25 ± 0.44
4r	**35.58 ± 0.34**	1088.76 ± 0.58
4s	47.96 ± 0.19	924.27 ± 0.32
4t	46.96 ± 0.42	119.50 ± 0.34
4u	**23.19 ± 0.23**	904.15 ± 0.46
4v	**21.27 ± 0.58**	**59.15 ± 0.29**
4w	112.09 ± 0.66	726.31 ± 0.41
4x	**27.30 ± 0.26**	231.09 ± 0.17
Ascorbic acid[b]	41.84 ± 0.25	90.10 ± 0.70

[a] SEM (standard error mean). [b] Standard for ABTS and DPPH radical scavenging activity. Bold values show the lowest IC_{50}s.

4v interacts with the receptor at active site-3 through conventional H-bonding, π–π stacked type of bond, carbon–hydrogen bonds, π–π T-shapes, and π-cation, alkyl, π-sigma, and π-alkyl types of bonds. Carbonyl oxygen atoms of the quinoline ring and indole ring of **4v** interact with TRP A:173 (2.88 Å) and HIS A:296 (4.67 Å) through conventional H-bonds and π–π stacked type of bond, respectively. An aryl ring of indole of **4a** interacts with ILE A:83 (5.49 Å), TYR A:174 (4.88 Å) and TRP A:173 (5.50 Å) through π-alkyl, π–π stacked and π–π T-shaped interactions, respectively. The methoxy group attached to the aryl ring of **4a** interacts with ILE A:83 (5.30 Å) and TYR A:174 (4.88 Å) through alkyl and π-sigma types of bonds, respectively. Furthermore, an aryl ring of 1,3-benzodioxol interacts with HIS A:296 (4.67 Å) and ARG A:19 (4.95 Å) through π–π T-shaped and π-cation types of bonds. These interactions make the binding of **4a** and **4v** strong enough in the binding sites of the *Listeria monocytogenes* targeted antioxidant protein of the LD-carboxypeptidase domain. So, **4a** and **4v** inhibit radical growth and show a good minimum inhibitory concentration value.

2.5. *In silico* ADME prediction

Prediction of absorption, distribution, metabolism, and excretion (ADME) properties before experimental trials is an essential aspect of the drug discovery and development process. The most potent antioxidants **4a** and **4v** were evaluated for *in silico* drug-likeness and ADME prediction. Several filters such as the Lipinski filter, Ghose filter, Veber filter, Egan filter and Muegge filter help predict drug-likeness based on their physicochemical properties. It was observed that both **4a** and **4v** obeyed all necessary rules and had no violation of such rules, proving them to be important drug candidate. The calculated physicochemical properties of potent compounds are summarized in Table S1 (mentioned in the ESI†).

The calculated bioavailability score was found to be 0.55 for **4a** and **4v**. BOILED-Egg delineation was used to predict high gastrointestinal absorption (HIA) and blood–brain barrier (BBB) permeability of **4a** and **4v**. BOILED-Egg delineation of these **4a** and **4v** is illustrated in Fig. 6 "*The white region is the physicochemical space of molecules with the highest probability of being absorbed by the gastrointestinal tract, and the yellow region (yolk) is the physicochemical* space *of molecules with the highest probability to permeate to the brain*".[32] **4v** shows high gastrointestinal absorbance, and it has no blood–brain permeability, while **4a** shows blood–brain permeability. Blue dots for **4a** and **4v** denoted that they are P-gp substrates. From the SVM model, **4a** was found to be a CYP1A2 inhibitor except for **4v**, whereas both **4a** and **4v** were found to be inhibitors of CYP2C19, CYP2C9, CYP2D6 and CYP3A4 which can perform metabolic biotransformation. Furthermore, there were no PAINS and Brenk filter alerts of toxicity found for **4a** and **4v**.

3. Experimental

3.1. General

All chemicals used in this synthesis are commercially available and used without further purification. Melting points were obtained by the open capillary tube method and are uncorrected. High-resolution mass spectra (HRMS) were acquired using an Agilent technologies model G6564 QTOF. Nuclear magnetic resonance spectra (^{1}H NMR & ^{13}C NMR) were obtained using a Bruker 500 MHz WB FT-NMR spectrometer having proton noise decoupling mode with a standard 5 mm probe using DMSO-d_6 solution. Abbreviations used for the ^{1}H NMR signal are as follows: s = singlet, d = doublet, t = triplet, q = quartet, qu = quintet, dd = double doublet, td = triple doublet, and m = multiplet. The chemical shifts are reported in parts per million and coupling constants (*J*) are provided in Hertz.

3.2. General procedure for the synthesis of spiroacridines 4a–p and spiroquinolines 4q–x

In a 50 mL round bottom flask, a mixture of 3,4-methylenedioxy aniline **1** (1 mmol), substituted isatins **2a–h** (1 mmol) and cyclic 1,3-diones **3a–c** (1 mmol) in 3 mL glacial acetic acid was refluxed for 5–8 min. On completion of the reaction (TLC), 5 mL of distilled water was added to the reaction mixture and stirred at room temperature for complete precipitation of the product. The furnished solid mass was filtered off, dried and then thoroughly washed again with 5 mL 5% ethyl acetate solution in *n*-hexane to afford the desired products **4a–x**.

3.2.1. 7′,7′-Dimethyl-7′,8′-dihydro-5′*H*-spiro[indoline-3,10′-[1,3]dioxolo[4,5-*b*]acridine]-2,9′(6′*H*)-dione (4a). White solid,

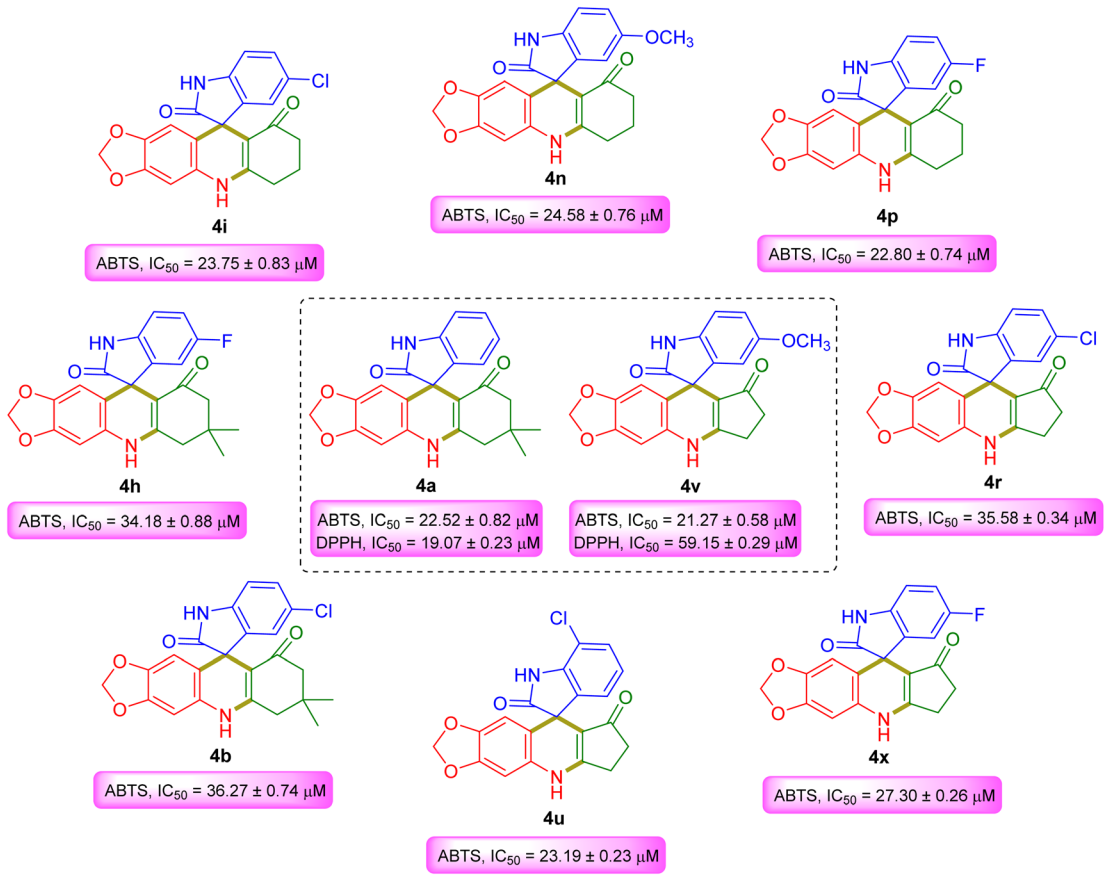

Fig. 4 Potent ABTS and DPPH radical scavengers.

mp greater than 300 °C; ^{1}H-NMR (500 MHz, DMSO-d$_6$) (δ, ppm): 10.25 (s, 1H, NH), 9.51 (s, 1H, NH), 7.08–7.05 (m, 1H, ArH), 6.81–6.76 (m, 3H, ArH), 6.52 (s, 1H, ArH), 5.97 (s, 1H, ArH), 5.90 (s, 1H, OCH$_a$H$_b$O), 5.86 (s, 1H, OCH$_b$H$_a$O), 2.50–2.36 (m, 2H, CH$_2$), 2.08 (d, J = 16 Hz, 1H, COCH$_a$H$_b$), 1.92 (d, J = 16 Hz, 1H, COCH$_b$H$_a$), 1.04 (s, 3H, CH$_3$), 0.99 (s, 3H, CH$_3$); ^{13}C-NMR (125 MHz, DMSO-d$_6$) (δ, ppm): 190.7, 179.7, 150.9, 145.6, 142.3, 140.0, 138.9, 128.7, 126.0, 121.7, 120.8, 114.6, 107.8, 104.2, 102.5, 100.1, 95.8, 50.2, 49.0, 39.5, 31.1, 27.4, 25.7; HRMS (ESI-MS) m/z calcd for $C_{23}H_{21}N_2O_4$ [M + H]$^+$: 389.1501, found: 389.1518.

3.2.2. 5-Chloro-7′,7′-dimethyl-7′,8′-dihydro-5′*H*-spiro[indoline-3,10′-[1,3]dioxolo[4,5-*b*]acridine]-2,9′(6′*H*)-dione (4b). Off-white solid, mp greater than 300 °C; ^{1}H-NMR (500 MHz, DMSO-d$_6$) (δ, ppm): 10.40 (s, 1H, NH), 9.60 (s, 1H, NH), 7.13 (dd, J = 8.2 Hz, 2.2 Hz, 1H, ArH), 6.83 (d, J = 8.2 Hz, 1H, ArH), 6.75 (d, J = 2.1 Hz, 1H, ArH), 6.55 (s, 1H, ArH), 5.97 (s, 1H, ArH), 5.93 (s, 1H, OCH$_a$H$_b$O), 5.88 (s, 1H, OCH$_b$H$_a$O), 2.46 (d, J = 4.5 Hz, 2H, CH$_2$), 2.07 (d, J = 16 Hz, 1H, COCH$_a$H$_b$), 1.98 (d, J = 16 Hz, 1H, COCH$_b$H$_a$), 1.04 (s, 3H, CH$_3$), 1.01 (s, 3H, CH$_3$); ^{13}C-NMR (125 MHz, DMSO-d$_6$) (δ, ppm): 190.9, 179.3, 151.3, 145.9, 142.5, 140.6, 139.1, 128.7, 126.0, 124.2, 121.6, 113.7, 109.3, 104.0, 101.9, 100.2, 96.0, 50.5, 48.9, 39.4, 31.2, 27.0, 26.1; HRMS (ESI-MS) m/z calcd for $C_{23}H_{19}ClN_2O_4$ [M]$^+$: 422.1033, found: 422.1038.

3.2.3. 5-Bromo-7′,7′-dimethyl-7′,8′-dihydro-5′*H*-spiro[indoline-3,10′-[1,3]dioxolo[4,5-*b*]acridine]-2,9′(6′*H*)-dione (4c). Off white solid, mp greater than 300 °C; ^{1}H-NMR (500 MHz, DMSO-d$_6$) (δ, ppm): 10.42 (s, 1H, NH), 9.60 (s, 1H, NH), 8.32 (s, 1H, ArH), 7.26 (dd, J = 8.5 Hz, 2 Hz, 1H, ArH), 6.86 (d, J = 2.0 Hz, 1H, ArH), 6.79 (d, J = 8.5 Hz, 1H, ArH), 6.55 (s, 1H, ArH), 5.98 (s, 1H, ArH), 5.93 (s, 1H, OCH$_a$H$_b$O), 5.88 (s, 1H, OCH$_b$H$_a$O), 2.46 (s, 2H, CH$_2$), 2.07 (d, J = 16 Hz, 1H, COCH$_a$H$_b$), 1.99 (d, J = 16 Hz, 1H, COCH$_b$H$_a$), 1.04 (s, 3H, CH$_3$), 1.01 (s, 3H, CH$_3$); ^{13}C-NMR (125 MHz, DMSO-d$_6$) (δ, ppm): 190.9, 179.2, 151.3, 145.9, 142.5, 141.0, 139.5, 128.8, 128.6, 124.3, 111.9, 109.9, 104.0, 101.9, 100.2, 96.0, 78.0, 48.9, 39.4, 31.1, 27.9, 27.0, 26.1; HRMS (ESI-MS) m/z calcd for $C_{23}H_{20}BrN_2O_4$ [M + H]$^+$: 467.0606, found: 467.0602.

3.2.4. 5,7′,7′-Trimethyl-7′,8′-dihydro-5′*H*-spiro[indoline-3,10′-[1,3]dioxolo[4,5-*b*]acridine]-2,9′(6′*H*)-dione (4d). White solid, mp greater than 300 °C; ^{1}H-NMR (500 MHz, DMSO-d$_6$) (δ, ppm): 10.14 (s, 1H, NH), 9.49 (s, 1H, NH), 6.86 (d, J = 8 Hz, 1H, ArH), 6.69 (d, J = 7.5 Hz, 1H, ArH), 6.57 (s, 1H, ArH), 6.51 (s, 1H, ArH), 5.95 (s, 1H, ArH), 5.90 (s, 1H, OCH$_a$H$_b$O), 5.86 (s, 1H, OCH$_b$H$_a$O), 2.11 (s, 2H, CH$_2$), 1.96–1.90 (m, 2H, CH$_2$), 1.29 (s, 3H, ArCH$_3$), 1.04 (s, 3H, CH$_3$), 1.00 (s, 3H, CH$_3$); ^{13}C-NMR (125 MHz, DMSO-d$_6$) (δ, ppm): 190.9, 179.3, 151.4, 146.0, 142.6, 141.1, 139.6, 128.9, 128.7, 124.4, 113.7, 112.0, 110.0, 104.1, 102.0, 100.3, 96.1, 49.0, 39.5, 31.2, 28.0, 27.6, 27.1, 26.2; HRMS

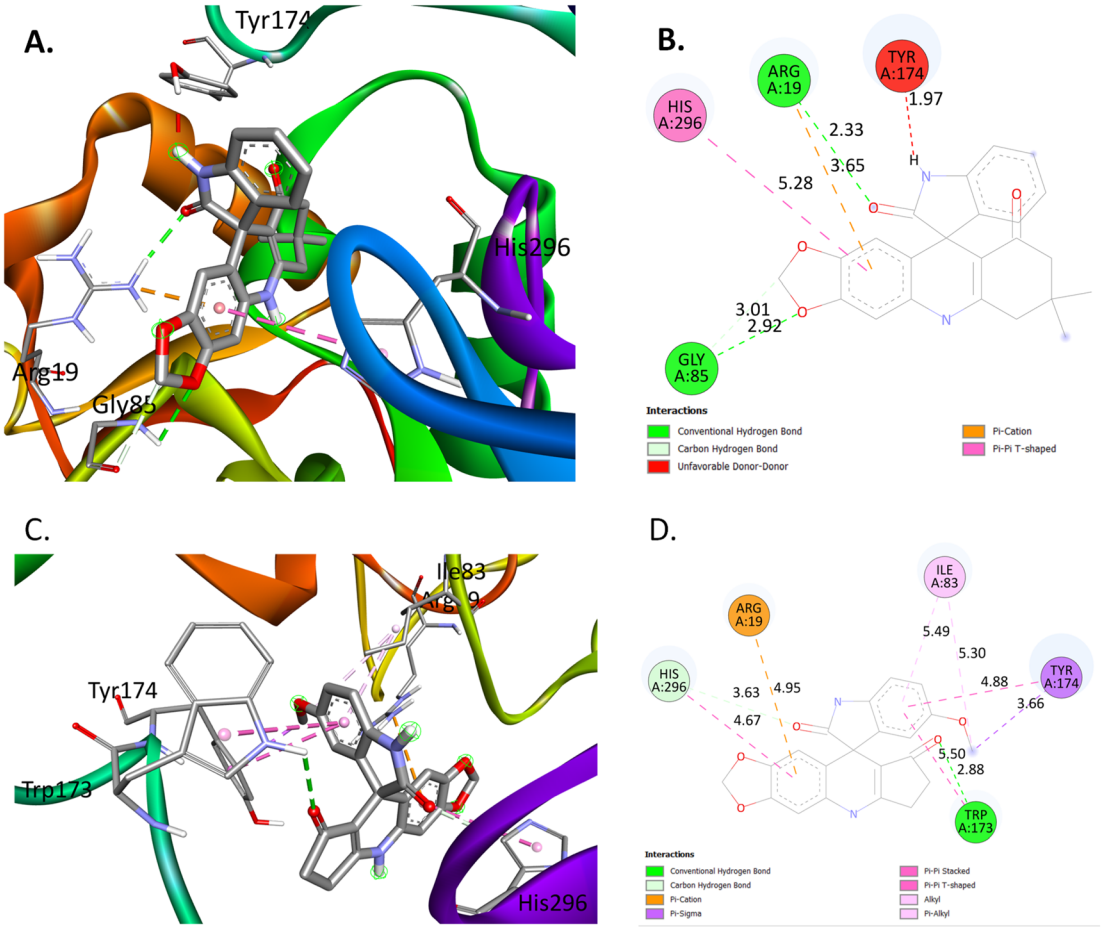

Fig. 5 Molecular docking study of **4a** and **4v**: (A) **4a** was docked on *Listeria monocytogenes* to identify the potential binding sites in the LD-carboxypeptidase domain; (B) interaction diagram of **4a**; (C) **4v** docked on *Listeria monocytogenes* to identify the potential binding sites in the LD-carboxypeptidase domain; (D) interaction diagram of **4v**.

(ESI-MS) *m*/*z* calcd for $C_{24}H_{23}N_2O_4$ $[M + H]^+$: 403.1658, found: 403.1654.

3.2.5. 7-Chloro-7′,7′-dimethyl-7′,8′-dihydro-5′*H*-spiro[indoline-3,10′-[1,3]dioxolo[4,5-*b*]acridine]-2,9′(6′*H*)-dione (4e). Off white solid, mp greater than 300 °C; ^{1}H-NMR (500 MHz, DMSO-d_6) (δ, ppm): 10.68 (s, 1H, NH), 9.61 (s, 1H, NH), 7.13 (d, J = 8 Hz, 1H, ArH), 6.82 (t, J = 8 Hz, 1H, ArH), 6.74 (d, J = 7 Hz, 1H, ArH), 6.54 (s, 1H, ArH), 5.97 (s, 1H, ArH), 5.92 (s, 1H, OCH_aH_bO), 5.87 (s, 1H, $OC\underline{H}_bH_aO$), 2.45 (m, 2H, CH_2), 2.09 (d, J = 16 Hz, 1H, $COCH_aH_b$), 1.93 (d, J = 16 Hz, 1H, $COCH_bH_a$), 1.04 (s, 3H, CH_3), 0.98 (s, 3H, CH_3); ^{13}C-NMR (125 MHz, DMSO-d_6) (δ, ppm): 192.3, 181.3, 152.5, 147.2, 143.9, 141.5, 140.5, 130.2, 127.6, 123.3, 122.0, 116.2, 109.4, 105.8, 104.1, 101.7, 97.4, 51.8, 50.6, 41.1, 32.6, 29.0, 27.3; HRMS (ESI-MS) *m*/*z* calcd for $C_{23}H_{19}ClN_2O_4$ $[M]^+$: 422.1033, found: 422.1038.

3.2.6. 5-Methoxy-7′,7′-dimethyl-7′,8′-dihydro-5′*H*-spiro[indoline-3,10′-[1,3]dioxolo[4,5-*b*]acridine]-2,9′(6′*H*)-dione (4f). Off white solid, mp greater than 300 °C; ^{1}H-NMR (500 MHz, DMSO-d_6) (δ, ppm): 10.08 (s, 1H, NH), 9.50 (s, 1H, NH), 6.72 (d, J = 8.5 Hz, 1H, ArH), 6.64 (d, J = 8.5 Hz, 1H, ArH), 6.52 (s, 1H, ArH), 6.33 (s, 1H, ArH), 5.98 (s, 1H, ArH), 5.91 (s, 1H, OCH_aH_bO), 5.87 (s, 1H, $OC\underline{H}_bH_aO$), 3.58 (s, 3H, OCH_3), 2.08 (d, J = 16 Hz, 1H, $COCH_aH_b$), 1.94 (d, J = 16 Hz, 1H, $COCH_bH_a$), 1.91 (s, 2H, CH_2), 1.04 (s, 3H, CH_3), 1.00 (s, 3H, CH_3); ^{13}C-NMR (125 MHz, DMSO-d_6) (δ, ppm): 192.0, 180.5, 152.5, 147.1, 143.6, 141.8, 140.3, 129.8, 127.1, 125.4, 122.8, 114.8, 110.5, 105.2, 103.1, 101.4, 97.2, 51.7, 50.1, 40.6, 32.3, 28.2, 27.3, 21.1; HRMS (ESI-MS) *m*/*z* calcd for $C_{24}H_{20}N_2O_4Na$ $[M + Na] + [-H_2O]$: 423.1321, found: 423.1113.

3.2.7. 7′,7′-Dimethyl-5-nitro-7′,8′-dihydro-5′*H*-spiro[indoline-3,10′-[1,3]dioxolo[4,5-*b*]acridine]-2,9′(6′*H*)-dione (4g). Greenish yellow solid, mp greater than 300 °C; ^{1}H-NMR (500 MHz, DMSO-d_6) (δ, ppm): 10.04 (s, 1H, NH), 9.75 (s, 1H, NH), 8.10 (dd, J = 8.5 Hz, 2.5 Hz, 1H, ArH), 7.57 (d, J = 2 Hz, 1H, ArH), 7.03 (d, J = 9 Hz, 1H, ArH), 6.58 (s, 1H, ArH), 6.00 (s, 1H, ArH), 5.93 (s, 1H, OCH_aH_bO), 5.89 (s, 1H, $OC\underline{H}_bH_aO$), 2.07 (d, J = 16 Hz, 1H, $COCH_aH_b$), 1.99 (d, J = 16 Hz, 1H, $COCH_bH_a$), 1.90 (s, 2H, CH_2), 1.04 (s, 3H, CH_3), 1.03 (s, 3H, CH_3); ^{13}C-NMR (125 MHz, DMSO-d_6) (δ, ppm): 191.4, 179.7, 151.8, 146.4, 143.0, 141.6, 140.0, 129.3, 129.2, 124.9, 114.2, 112.4, 110.4, 104.5, 102.5, 100.7, 96.5, 49.4, 39.9, 31.6, 28.4, 27.5, 26.6; HRMS (ESI-MS) *m*/*z* calcd for $C_{23}H_{19}N_3O_6$ $[M]^+$: 433.1274, found: 433.1240.

3.2.8. 5-Fluoro-7′,7′-dimethyl-7′,8′-dihydro-5′*H*-spiro[indoline-3,10′-[1,3]dioxolo[4,5-*b*]acridine]-2,9′(6′*H*)-dione (4h).

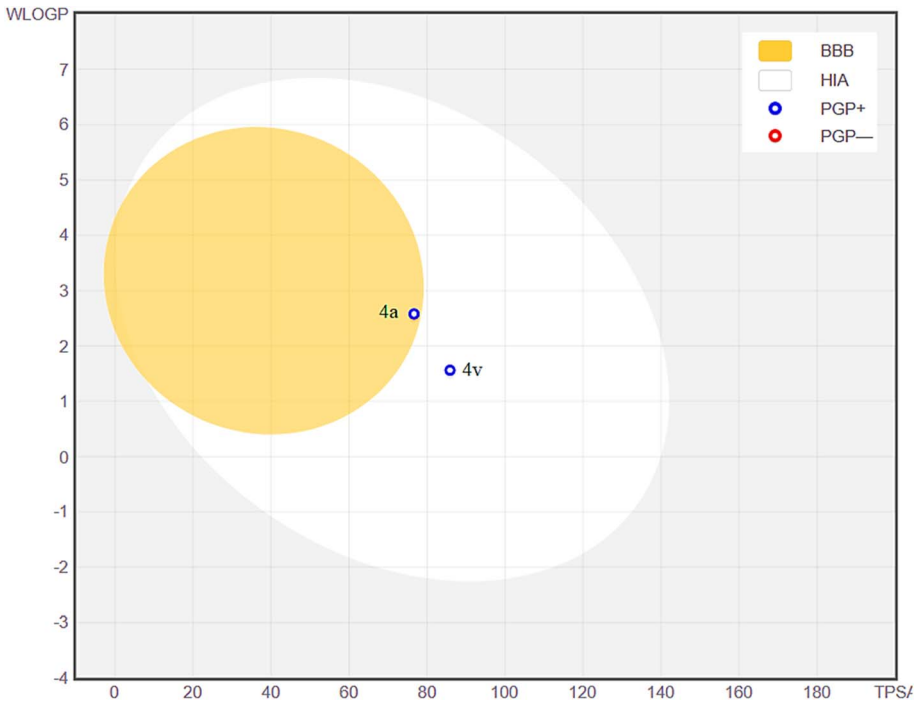

Fig. 6 BOILED Egg model of compounds **4a** and **4v**.

White solid, mp greater than 300 °C; ^{1}H-NMR (500 MHz, DMSO-d_6) (δ, ppm): 10.27 (s, 1H, NH), 9.57 (s, 1H, NH), 6.92–6.88 (m, 1H, ArH), 6.81–6.78 (m, 1H, ArH), 6.60 (dd, J = 8 Hz, 2.5 Hz, 1H, ArH), 6.53 (s, 1H, ArH), 5.97 (s, 1H, ArH), 5.92 (s, 1H, OCH_aH$_b$O), 5.87 (s, 1H, OC$\underline{H}_b$H$_a$O), 2.44 (m, 2H, CH_2), 2.07 (d, J = 16 Hz, 1H, COCH_aH$_b$), 1.96 (d, J = 16 Hz, 1H, COCH_bH$_a$), 1.04 (s, 3H, CH_3), 1.00 (s, 3H, CH_3); ^{13}C-NMR (125 MHz, DMSO-d_6) (δ, ppm):192.5, 181.1, 159.3, 157.5, 154.4, 147.2, 143.7, 141.9 (d, J = 25 Hz), 137.7, 130.0, 115.2, 113.5 (d, J = 90 Hz), 110.8 (d, J = 95 Hz), 109.7 (d, J = 30 Hz), 105.4, 104.8, 101.5, 97.3, 62.3, 52.2, 36.8, 27.6, 25.8, 21.3; HRMS (ESI-MS) m/z calcd for $C_{23}H_{20}FN_2O_4$ [M + H]$^+$: 407.1407, found: 407.1393.

3.2.9. 7′,8′-Dihydro-5′*H*-spiro[indoline-3,10′-[1,3]dioxolo [4,5-*b*]acridine]-2,9′(6′*H*)-dione (4i). Off white solid, mp greater than 300 °C; ^{1}H-NMR (500 MHz, DMSO-d_6) (δ, ppm): 10.24 (s, 1H, NH), 9.54 (s, 1H, NH), 7.08–7.04 (m, 1H, ArH), 6.80–6.77 (m, 3H, ArH), 6.52 (s, ArH), 5.95 (s, 1H, ArH), 5.90 (s, 1H, OCH_aH$_b$O), 5.85 (s, 1H, OC$\underline{H}_b$H$_a$O), 2.57 (t, J = 6 Hz, 2H, CH_2), 2.05–2.18 (m, 2H, CH_2), 1.83–1.92 (m, 2H, CH_2); ^{13}C-NMR (125 MHz, DMSO-d_6) (δ, ppm): 192.6, 181.4, 154.4, 147.2, 143.8, 141.5, 140.6, 130.1, 127.6, 123.5, 121.9, 116.2, 109.4, 105.5, 101.7, 97.5, 97.2, 51.9, 37.1, 27.8, 21.5; HRMS (ESI-MS) m/z calcd for $C_{21}H_{16}N_2O_4$ [M]$^+$: 360.1110, found: 360.1110.

3.2.10. 5-Chloro-7′,8′-dihydro-5′*H*-spiro[indoline-3,10′-[1,3] dioxolo[4,5-*b*]acridine]-2,9′(6′*H*)-dione (4j). Light pink, mp greater than 300 °C; ^{1}H-NMR (500 MHz, DMSO-d_6) (δ, ppm): 10.40 (s, 1H, NH), 9.64 (s, 1H, NH), 7.13 (dd, J = 8 Hz, 2 Hz, 1H, ArH), 6.83 (d, J = 8.5 Hz, 1H, ArH), 6.79 (d, J = 2.5 Hz, 1H, ArH), 6.53 (s, 1H, ArH), 5.96 (s, 1H, ArH), 5.92 (s, 1H, OCH_aH$_b$O), 5.87 (s, 1H, OC$\underline{H}_b$H$_a$O), 3.77 (qu, J = 12 Hz, 6 Hz, 2H, CH_2), 2.58 (dd, J = 11 Hz, 5 Hz, 2H, CH_2), 2.16–2.12 (m, 2H, CH_2); ^{13}C-NMR (125 MHz, DMSO-d_6) (δ, ppm): 179.5, 153.2, 145.9, 142.4, 140.7, 139.0, 128.5, 125.9, 124.2, 121.8, 113.6, 109.3, 103.9, 103.3, 100.2, 95.9, 60.9, 50.5, 35.4, 26.1, 24.3, 19.9; HRMS (ESI-MS) m/z calcd for $C_{21}H_{15}ClN_2O_4$ [M]$^+$: 394.0720, found: 394.0734.

3.2.11. 5-Bromo-7′,8′-dihydro-5′*H*-spiro[indoline-3,10′-[1,3] dioxolo[4,5-*b*]acridine]-2,9′(6′*H*)-dione (4k). Off white solid, mp greater than 300 °C; ^{1}H-NMR (500 MHz, DMSO-d_6) (δ, ppm): 10.41 (s, 1H, NH), 9.63 (s, 1H, NH), 7.26 (dd, J = 8.5 Hz, 2 Hz, 1H, ArH), 6.90 (d, J = 2 Hz, 1H, ArH), 6.78 (d, J = 8 Hz, 1H, ArH), 6.55 (s, 1H, ArH), 5.97 (s, 1H, ArH), 5.92 (s, 1H, OCH_aH$_b$O), 5.88 (s, 1H, OC$\underline{H}_b$H$_a$O), 3.78 (qu, J = 6 Hz, 2.5 Hz, 1H, 2H, CH_2), 2.59 (dd, J = 12 Hz, 5.5 Hz, 2H, CH_2), 2.17–2.12 (m, 2H, CH_2); ^{13}C-NMR (125 MHz, DMSO-d_6) (δ, ppm): 191.2, 179.3, 153.2, 145.9, 142.4, 141.2, 139.4, 128.8, 128.5, 124.5, 113.7, 112.0, 109.8, 104.0, 103.3, 100.2, 95.9, 50.5, 35.4, 26.1, 24.3, 19.9; HRMS (ESI-MS) m/z calcd for $C_{21}H_{16}BrN_2O_4$ [M + H]$^+$: 439.0293, found: 439.0289.

3.2.12. 5-Methyl-7′,8′-dihydro-5′*H*-spiro[indoline-3,10′-[1,3] dioxolo[4,5-*b*]acridine]-2,9′(6′*H*)-dione (4l). Off white solid, mp greater than 300 °C; ^{13}C-NMR (125 MHz, DMSO-d_6) (δ, ppm): 191.1, 179.3, 153.2, 145.8, 142.4, 141.1, 139.4, 128.8, 128.5, 124.4, 113.6, 111.9, 109.8, 103.9, 103.3, 100.1, 95.9, 60.9, 50.5, 35.3, 26.1, 24.3, 19.8; HRMS (ESI-MS) m/z calcd for $C_{22}H_{19}N_2O_4$ [M + H]$^+$: 375.1345, found: 375.1343.

3.2.13. 7-Chloro-7′,8′-dihydro-5′*H*-spiro[indoline-3,10′-[1,3] dioxolo[4,5-*b*]acridine]-2,9′(6′*H*)-dione (4m). Brownish black solid, mp greater than 300 °C; ^{1}H-NMR (500 MHz, DMSO-d_6) (δ, ppm): 10.68 (s, 1H, NH), 9.65 (s, 1H, NH), 7.14 (dd, J = 8 Hz, 1 Hz, 1H, ArH), 6.82 (t, J = 7.5 Hz, 1H, ArH), 6.76 (d, J = 7 Hz, 1H, ArH), 6.55 (s, 1H, ArH), 5.96 (s, 1H, ArH), 5.93 (s, 1H, OCH_aH$_b$O), 5.88 (s, 1H, OC$\underline{H}_b$H$_a$O), 2.59 (t, J = 6.5 Hz, 2H, CH_2), 2.21–2.07 (m, 2H, CH_2), 1.94–1.84 (m, 2H, CH_2); ^{13}C-NMR (125 MHz,

DMSO-d_6) (δ, ppm): 179.6, 153.3, 145.9, 142.5, 140.8, 139.0, 128.6, 126.0, 124.3, 121.8, 113.7, 109.3, 104.0, 103.3, 100.2, 96.0, 61.0, 50.6, 35.4, 26.2, 24.3; HRMS (ESI-MS) *m*/*z* calcd for $C_{21}H_{15}ClN_2O_4$ $[M + H]^+$: 395.0799, found: 395.0796.

3.2.14. 5-Methoxy-7′,8′-dihydro-5′*H*-spiro[indoline-3,10′-[1,3]dioxolo[4,5-*b*]acridine]-2,9′(6′*H*)-dione (4n). White solid, mp greater than 300 °C; ^{1}H-NMR (500 MHz, DMSO-d_6) (δ, ppm): 10.07 (s, 1H, NH), 9.52 (s, 1H, NH), 6.71 (d, J = 8.5 Hz, 1H, ArH), 6.64 (dd, J = 8 Hz, 2.5 Hz, 1H, ArH), 6.51 (s, 1H, ArH), 6.36 (d, J = 2.5 Hz, 1H, ArH), 5.96 (s, 1H, ArH), 5.90 (s, 1H, OCH_aH_bO), 5.86 (s, 1H, $OC\underline{H}_bH_aO$), 3.59 (s, 1H, OCH_3), 2.57 (t, J = 5.5 Hz, 2H, CH_2), 2.15–2.07 (m, 2H, CH_2), 1.91–1.88 (m, 2H, CH_2); ^{13}C-NMR (125 MHz, DMSO-d_6) (δ, ppm): 192.8, 180.9, 154.8, 147.4, 144.0, 142.8, 141.0, 130.4, 130.1, 126.1, 115.2, 113.6, 111.4, 110.1, 105.6, 104.9, 101.8, 97.5, 62.5, 52.1, 37.0, 25.9, 21.5; HRMS (ESI-MS) *m*/*z* calcd for $C_{22}H_{18}N_2O_5$ $[M]^+$: 390.1216, found: 390.1179.

3.2.15. 5-Nitro-7′,8′-dihydro-5′*H*-spiro[indoline-3,10′-[1,3]dioxolo[4,5-*b*]acridine]-2,9′(6′*H*)-dione (4o). Light brown solid, mp greater than 300 °C; ^{1}H-NMR (500 MHz, DMSO-d_6) (δ, ppm): 11.04 (s, 1H, NH), 9.77 (s, 1H, NH), 8.09 (dd, J = 8.5 Hz, 2 Hz, 1H, ArH), 7.61 (d, J = 2 Hz, 1H, ArH), 7.02 (d, J = 8.5 Hz, 1H, ArH), 6.58 (s, 1H, ArH), 5.99 (s, 1H, ArH), 5.92 (s, 1H, OCH_aH_bO), 5.88 (s, 1H, $OC\underline{H}_bH_aO$), 2.67–2.57 (m, 2H, CH_2), 2.18–2.09 (m, 2H, CH_2), 1.90–1.88 (m, 2H, CH_2); ^{13}C-NMR (125 MHz, DMSO-d_6) (δ, ppm): 193.0, 181.7, 155.2, 148.5, 147.7, 144.2, 142.6, 141.0, 130.2, 125.4, 118.6, 114.5, 109.6, 105.5, 104.6, 101.9, 97.7, 51.9, 36.8, 27.7, 21.4; HRMS (ESI-MS) *m*/*z* calcd for $C_{21}H_{16}N_3O_6$ $[M + H]^+$: 406.1039, found: 406.1037.

3.2.16. 5-Fluoro-7′,8′-dihydro-5′*H*-spiro[indoline-3,10′-[1,3]dioxolo[4,5-*b*]acridine]-2,9′(6′*H*)-dione (4p). White solid, mp greater than 300 °C; ^{1}H-NMR (500 MHz, DMSO-d_6) (δ, ppm): 10.28 (s, 1H, NH), 9.60 (s, 1H, NH), 6.92–6.87 (m, 1H, ArH), 6.78 (dd, J = 8.5 Hz, 4 Hz, 1H, ArH), 6.64 (dd, J = 8 Hz, 2.5 Hz, 1H, ArH), 6.53 (s, 1H, ArH), 5.96 (s, 1H, ArH), 5.91 (s, 1H, OCH_aH_bO), 5.87 (s, 1H, $OC\underline{H}_bH_aO$), 3.77 (qu, J = 12 Hz, 6 Hz, 2H, CH_2), 2.57 (t, J = 6 Hz, 2H, CH_2), 2.15–2.08 (m, 2H, CH_2); ^{13}C-NMR (125 MHz, DMSO-d_6) (δ, ppm): 192.6, 181.3, 159.5, 157.7, 154.6, 147.4, 143.9, 142.1 (d, J = 30 Hz), 137.9, 130.1, 115.4, 113.7 (d, J = 95 Hz), 111.0 (d, J = 100 Hz), 109.9 (d, J = 35 Hz), 105.6, 105.0, 101.7, 97.5, 52.4, 37.0, 26.0, 21.5; HRMS (ESI-MS) *m*/*z* calcd for $C_{21}H_{16}FN_2O_4$ $[M + H]^+$: 379.1094, found: 379.1090.

3.2.17. 6,7-Dihydrospiro[cyclopenta[*b*][1,3]dioxolo[4,5-*g*]quinoline-9,3′-indoline]-2′,8(5*H*)-dione (4q). Off white solid, mp greater than 300 °C; ^{1}H-NMR (500 MHz, DMSO-d_6) (δ, ppm): 10.38 (s, 1H, NH), 10.15 (s, 1H, NH), 7.15 (t, J = 7.5 Hz, 1H, ArH), 6.87–6.81 (m, 3H, ArH), 6.58 (s, 1H, ArH), 5.94 (s, 1H, ArH), 5.90 (s, 2H, OCH_2O), 2.73 (d, J = 5.5 Hz, 2H, CH_2), 2.22 (d, J = 5.5 Hz, 2H, CH_2); ^{13}C-NMR (125 MHz, DMSO-d_6) (δ, ppm): 198.0, 178.5, 165.3, 146.8, 143.3, 139.9, 139.0, 130.8, 127.3, 125.2, 123.5, 114.1, 110.3, 107.5, 105.5, 101.0, 97.1, 50.6, 32.3, 25.0; HRMS (ESI-MS) *m*/*z* calcd for $C_{20}H_{15}N_2O_4$ $[M + H]^+$: 347.1032, found: 347.1043.

3.2.18. 5′-Chloro-6,7-dihydrospiro[cyclopenta[*b*][1,3]dioxolo[4,5-*g*]quinoline-9,3′-indoline]-2′,8(5*H*)-dione (4r). Off white solid, mp greater than 300 °C; ^{1}H-NMR (500 MHz, DMSO-d_6) (δ, ppm): 10.53 (s, 1H, NH), 10.22 (s, 1H, NH), 7.20 (dd, J = 8.5 Hz, 2 Hz, 1H, ArH), 6.88 (d, J = 8 Hz, 1H, ArH), 6.84 (d, J = 2.5 Hz, 1H, ArH), 6.60 (s, 1H, ArH), 5.96 (s, 1H, OCH_aH_bO), 5.94 (s, 1H, ArH), 5.92 (s, 1H, $OC\underline{H}_bH_aO$), 2.73 (dd, J = 10.5 Hz, 4.5 Hz, 2H, CH_2), 2.23 (t, J = 5 Hz, 2H, CH_2); ^{13}C-NMR (125 MHz, DMSO-d_6) (δ, ppm): 199.0, 179.5, 166.3, 147.8, 144.3, 140.9, 131.8, 128.3, 126.2, 124.5, 115.1, 111.3, 108.5, 106.5, 102.0, 98.1, 51.6, 33.3, 26.0; HRMS (ESI-MS) *m*/*z* calcd for $C_{20}H_{14}ClN_2O_4$ $[M + H]^+$: 381.0642, found: 381.0641.

3.2.19. 5′-Bromo-6,7-dihydrospiro[cyclopenta[*b*][1,3]dioxolo[4,5-*g*]quinoline-9,3′-indoline]-2′,8(5*H*)-dione (4s). Light brown solid, mp greater than 300 °C; ^{1}H-NMR (500 MHz, DMSO-d_6) (δ, ppm): 10.57 (s, 1H, NH), 10.54 (s, 1H, NH), 7.33 (dd, J = 8 Hz, 2 Hz, 1H, ArH), 6.94 (d, J = 2 Hz, 1H, ArH), 6.84 (d, J = 8.5 Hz, 1H, ArH), 6.60 (s, 1H, ArH), 5.95 (s, 1H, OCH_aH_bO), 5.94 (s, 1H, ArH), 5.92 (s, 1H, $OC\underline{H}_bH_aO$), 2.72 (t, J = 8.5 Hz, 2H, CH_2), 2.23 (t, J = 5 Hz, 2H, CH_2); ^{13}C-NMR (125 MHz, DMSO-d_6) (δ, ppm): 197.5, 177.8, 164.8, 146.2, 142.7, 139.7, 138.8, 130.2, 129.5, 125.6, 113.5, 112.4, 110.3, 106.9, 104.9, 100.4, 96.5, 49.9, 31.7, 23.1; HRMS (ESI-MS) *m*/*z* calcd for $C_{20}H_{14}BrN_2O_4$ $[M + H]^+$: 425.0136, found: 425.0133.

3.2.20. 5′-Methyl-6,7-dihydrospiro[cyclopenta[*b*][1,3]dioxolo[4,5-*g*]quinoline-9,3′-indoline]-2′,8(5*H*)-dione (4t). Light brown, mp greater than 300 °C; ^{1}H-NMR (500 MHz, DMSO-d_6) (δ, ppm): 10.29 (s, 1H, NH), 10.15 (s, 1H, NH), 6.93 (d, J = 7.5 Hz, 1H, ArH), 6.74 (d, J = 7.5 Hz, 1H, ArH), 6.62 (s, 1H, ArH), 6.57 (s, 1H, ArH), 5.93 (s, 1H, OCH_aH_bO), 5.90 (s, 1H, $OC\underline{H}_bH_aO$), 5.88 (s, 1H, ArH), 2.71 (dd, J = 10 Hz, 4.5 Hz, 2H, CH_2), 2.22–2.20 (m, 2H, CH_2), 2.14 (s, 3H, CH_3); ^{13}C-NMR (125 MHz, DMSO-d_6) (δ, ppm): 199.0, 179.8, 166.1, 147.5, 144.1, 139.3, 138.5, 131.7, 131.2, 128.6, 125.0, 116.1, 109.5, 109.2, 106.6, 101.9, 97.4, 51.4, 33.4, 24.6, 21.1; HRMS (ESI-MS) *m*/*z* calcd for $C_{21}H_{17}N_2O_4$ $[M + H]^+$: 361.1188, found: 361.1189.

3.2.21. 7′-Chloro-6,7-dihydrospiro[cyclopenta[*b*][1,3]dioxolo[4,5-*g*]quinoline-9,3′-indoline]-2′,8(5*H*)-dione (4u). Off white solid, mp greater than 300 °C; ^{1}H-NMR (500 MHz, DMSO-d_6) (δ, ppm): 10.85 (s, 1H, NH), 10.26 (s, 1H, NH), 7.22 (d, J = 8.5 Hz, 1H, ArH), 6.88 (t, J = 7.5 Hz, 1H, ArH), 6.79 (d, J = 7.5 Hz, 1H, ArH), 6.60 (s, 1H, ArH), 5.95 (s, 1H, OCH_aH_bO), 5.94 (s, 1H, ArH), 5.91 (s, 1H, $OC\underline{H}_bH_aO$), 2.73 (t, J = 5 Hz, 2H, CH_2), 2.43–2.21 (m, 2H, CH_2); ^{13}C-NMR (125 MHz, DMSO-d_6) (δ, ppm):199.0, 179.6, 166.2, 147.8, 144.3, 139.7, 131.7, 128.4, 123.7, 123.2, 115.2, 114.0, 108.7, 106.5, 102.0, 98.1, 79.6, 52.2, 33.3, 24.7; HRMS (ESI-MS) *m*/*z* calcd for $C_{20}H_{14}ClN_2O_4$ $[M + H]^+$: 381.0642, found: 381.0677.

3.2.22. 5′-Methoxy-6,7-dihydrospiro[cyclopenta[*b*][1,3]dioxolo[4,5-*g*]quinoline-9,3′-indoline]-2′,8(5*H*)-dione (4v). Light brown solid, mp greater than 300 °C; ^{1}H-NMR (500 MHz, DMSO-d_6) (δ, ppm): 10.22 (s, 1H, NH), 10.16 (s, 1H, NH), 6.79 (d, J = 8.5 Hz, 1H, ArH), 6.74–6.71 (m, 1H, ArH), 6.58 (s, 1H, ArH), 6.39 (d, J = 2.5 Hz, 1H, ArH), 5.94 (s, 1H, OCH_aH_bO), 5.91 (s, 1H, $OC\underline{H}_bH_aO$), 5.90 (s, 1H, ArH), 3.61 (s, 3H, OCH_3), 2.74–2.70 (m, 2H, CH_2), 2.22 (t, J = 5 Hz, 2H, CH_2); ^{13}C-NMR (125 MHz, DMSO-d_6) (δ, ppm): 199.0, 179.7, 166.2, 155.6, 147.5, 144.1, 139.5, 135.2, 131.7, 115.9, 112.8, 111.4, 110.1, 109.0, 106.5, 101.9, 98.0, 55.8, 51.8, 33.4, 24.6; HRMS (ESI-MS) *m*/*z* calcd for $C_{21}H_{20}N_3O_5$ $[M + NH_4]^+$: 394.1403, found: 394.1426.

3.2.23. 5′-Nitro-6,7-dihydrospiro[cyclopenta[*b*][1,3]dioxolo[4,5-*g*]quinoline-9,3′-indoline]-2′,8(5*H*)-dione (4w). Off white solid, mp greater than 300 °C; ^{1}H-NMR (500 MHz, DMSO-d_6) (δ, ppm): 10.56 (s, 1H, NH), 10.23 (s, 1H, NH), 7.32 (dd, J = 8.5 Hz,

2 Hz, 1H, ArH), 6.94 (d, J = 1.5 Hz, 1H, ArH), 6.83 (d, J = 8 Hz, 1H, ArH), 6.59 (s, 1H, ArH), 5.95 (s, 1H, OCH_aH_bO), 5.94 (s, 1H, ArH), 5.91 (s, 1H, $OC\underline{H}_bH_aO$), 2.71 (t, J = 7.5 Hz, 2H, CH_2), 2.3 (t, J = 5 Hz, 2H, CH_2); ^{13}C-NMR (125 MHz, DMSO-d_6) (δ, ppm): 198.3, 179.0, 165.5, 154.9, 146.8, 143.4, 138.8, 134.5, 131.0, 115.2, 112.1, 110.7, 109.4, 108.3, 105.8, 101.2, 97.3, 55.1, 32.7, 23.9; HRMS (ESI-MS) m/z calcd for $C_{20}H_{14}N_3O_6$ $[M + H]^+$: 392.0883, found: 392.0882.

3.2.24. 5′-Fluoro-6,7-dihydrospiro[cyclopenta[*b*][1,3]dioxolo[4,5-*g*]quinoline-9,3′-indoline]-2′,8(5*H*)-dione (4x). Off white solid, mp greater than 300 °C; ^{1}H-NMR (500 MHz, DMSO-d_6) (δ, ppm): 10.43 (s, 1H, NH), 10.22 (s, 1H, NH), 7.00–6.96 (m, 1H, ArH), 6.85 (dd, J = 8.5 Hz, 4.5 Hz, 1H, ArH), 6.69 (dd, J = 7.5 Hz, 2 Hz, 1H, ArH), 6.59 (s, 1H, ArH), 5.95 (s, 1H, ArH), 5.92 (s, 2H, OCH_2O), 2.72 (d, J = 4 Hz, 2H, CH_2), 2.22 (d, J = 3 Hz, 2H, CH_2); ^{13}C-NMR (125 MHz, DMSO-d_6) (δ, ppm): 197.4, 178.2, 164.7, 146.1, 142.6, 138.1, 136.5, 130.2, 130.6, 113.6, 113.0 (d, J = 95 Hz), 110.5 (d, J = 95 Hz), 108.9 (d, J = 30 Hz), 107.0, 104.9, 100.4, 96.5, 78.0, 50.3, 31.7, 23.1; HRMS (ESI-MS) m/z calcd for $C_{20}H_{14}FN_2O_4$ $[M + H]^+$: 365.0938, found: 365.0937.

3.3. Computational details

The Gaussian 16 software package[33] was utilized for computational investigations and all DFT calculations were performed using the B3LYP method with a 6-311G+(d,p) basis set in the ground state. The chemical reactivity and stability of the molecule were investigated using Becke's three parameter (B3LYP) diffusion functionals at the 6-311G+(d,p) basis set. The frontier molecular orbital (FMO) and molecule electrostatic potential (MEP) surface analyses were accomplished by the DFT/B3LYP method using a 6-311G+(d,p) basis set. The orbital energy gap (E_{gap}) and other quantum chemical descriptors (QCDs) were calculated from frontier molecular orbitals (FMOs) with the same conceptual method and by using well-known equations. Gauss view 6.1.1 (ref. 34) was used for geometry optimization and data visualization.

3.4. ABTS radical scavenging assay

The ABTS free radical cation scavenging activity of compounds was determined by a standard procedure. First, a 7 mM concentrated solution of ABTS was prepared and then a 2.45 mM concentrated solution of potassium persulfate was added to the ABTS solution. After adding potassium persulfate to the ABTS solution, the solution was kept in a dark place for 12–16 h at room temperature. The sample solutions of the test compound were prepared in absolute alcohol ranging from 0.01 mg mL^{-1} to 1 mg mL^{-1}. Then the test sample was added to the ABTS solution and incubated for 30 min at 37 °C. The absorbance was measured at a wavelength of 734 nm, and the procedure was repeated for ascorbic acid as a reference standard. The % inhibition of radical scavenging activity was determined using the given formula.

$$\%\ \text{inhibition} = \frac{A_{\text{control}} - A_{\text{sample}}}{A_{\text{control}}} \times 100$$

3.5. DPPH radical scavenging assay

The free radical scavenging activity of DPPH was tested using a standard procedure. 0.3 mM DPPH concentrated solution in ethanol was incubated for 30 min at 37 °C with various test samples. The absorption of the sample was taken at 517 nm. The same procedure was followed for ascorbic acid as for the standard. The % inhibition of radical scavenging activity was determined using the given formula.

$$\%\ \text{inhibition} = \frac{A_{\text{control}} - A_{\text{sample}}}{A_{\text{control}}} \times 100$$

3.6. *In silico* molecular docking

3.6.1. Molecular docking. The AlphaFold structure of the *Listeria monocytogenes* targeted antioxidant protein of the LD-carboxypeptidase domain (ID: AF-A0A823DAK7-F1-model_v4) was imported from the AlphaFold Protein Structure Database (**https://alphafold.ebi.ac.uk/entry/A0A823DAK7**, 11/01/2024, 01:26 PM) (ebi.ac.uk). Autodock Vina software[35] was used for molecular docking simulations of **4a** and **4v**. Autodock Tools version 1.5.7 is used for pre-processing. In order to analyze the bound conformations and interactions, Discovery Studio Visualizer was used.

3.6.2. Ligand preparation for docking study. ChemBio3D 22.0.0 was used to draw the 3D structure of spiroacridine **4a** and spiroquinoline **4v**. The energy was minimized to a minimum RMS gradient of 0.000 in each interaction. All structures were saved in SDFile (*.sdf and *.sd) file format which was then transformed into a .pdb file using Open Babel for input to the Autodock tool. The ligand structure was then saved in the (.pdbqt) file format.

3.6.3. Preparation of the protein structure. The AlphaFold crystal structure of the *Listeria monocytogenes* targeted antioxidant protein of the LD-carboxypeptidase domain (ID: AF-A0A823DAK7-F1-model_v4) with the per-residue model confidence score (pLDDT) between 0 and 100 was imported (as .pdb file) from the AlphaFold Protein Structure Database (**https://alphafold.ebi.ac.uk/entry/A0A823DAK7**, 11/01/2024, 01:26 PM) (ebi.ac.uk). A circle with a volume of 20 × 20 × 20 Å^3 at centre 9.637000, 4.581000, and −0.419000 (site-1) and −0.363000, 8.831000, and −4.919 (site-3) were set as the grid. As the AlphaFold structure of LD-carboxypeptidase was free from crystal water, polar hydrogens were added with the help of Discovery Studio Visualizer. Finally, with the help of ADT, Kolmann and Gasteiger charges were added to each atom of protein and merged with the non-polar hydrogen atoms to form the protein structure. Then, the structure was saved in PDBQT file format.

3.7. *In silico* ADMET prediction

In silico ADMET prediction of the most potent antioxidants **4a** and **4q** were calculated using web tool SwissADME (**http://www.swissadme.ch/**).[36]

4. Conclusion

In conclusion, we have developed a green synthetic approach for the synthesis of spiroacridines and spiroquinolines *via*

a multicomponent reaction of 3,4-methylenedioxyaniline, isatin and cyclic 1,3-diones in glacial acetic acid. The key features of this protocol are the metal-free multicomponent approach, mild reaction conditions, faster reaction time, moderate to good yield and easy product purification without column chromatography. FMOs, various QCDs and MEP of all spiro molecules were obtained using DFT calculations using the B3LYP method with a 6-311G+(d,p) basis set. Furthermore, the antioxidant properties of all newly synthesized compounds were evaluated. According to *in silico* molecular docking studies of the most potent **4a** and **4v** with the targeted antioxidant protein, LD-carboxypeptidase, they show a strong binding affinity of −10.5 kcal mol^{-1} and −10.7 kcal mol^{-1}, respectively. In addition, **4a** and **4v** are the most potent radical scavengers as they possess good drug-likeness as well as *in silico* ADME prediction.

Conflicts of interest

The authors declare no conflict of interest.

Acknowledgements

SGP, PJP, DBU and HMP are grateful to the Department of Chemistry, Sardar Patel University, for providing computational & lab facilities. SGP is grateful to the UGC, New Delhi, for a UGC-JRF (NTA Ref. No. 201610157514; dated: 01.04.2021). MPP and DBU are thankful to the Knowledge Consortium of Gujarat for the SHODH fellowship (Student Reference No. 2021016434 & 2021016413, respectively).

References

1 P. J. Patel, S. G. Patel, D. B. Upadhyay, L. Ravi, A. Dhanasekaran and H. M. Patel, *RSC Adv.*, 2023, **13**, 24466–24473.
2 A. Lozynskyi, V. Zasidko, D. Atamanyuk, D. Kaminskyy, H. Derkach, O. Karpenko, V. Ogurtsov, R. Kutsyk and R. Lesyk, *Mol. Diversity*, 2017, **21**, 427–436.
3 E. N. Bentz, A. B. Pomilio and R. M. J. C. Lobayan, *Comput. Theor. Chem.*, 2017, **1110**, 14–24.
4 U. Asmat, K. Abad and K. Ismail, *Saudi Pharm. J.*, 2016, **24**, 547–553.
5 A. Sarkar, S. Santra, S. K. Kundu, A. Hajra, G. V. Zyryanov, O. N. Chupakhin, V. N. Charushin and A. Majee, *Green Chem.*, 2016, **18**, 4475–4525.
6 D. M. Patel and H. M. Patel, *ACS Sustain. Chem. Eng.*, 2019, **7**, 18667–18676.
7 B. H. Rotstein, S. Zaretsky, V. Rai and A. K. Yudin, *Chem. Rev.*, 2014, **114**, 8323–8359.
8 D. M. Patel, R. M. Vala, M. G. Sharma, D. P. Rajani and H. M. Patel, *ChemistrySelect*, 2019, **4**, 1031–1041.
9 E. Vitaku, D. T. Smith and J. T. Njardarson, *J. Med. Chem.*, 2014, **57**, 10257–10274.
10 M. M. M. Lobe and S. M. N. Efange, *R. Soc. Open Sci.*, 2020, **7**, 191316.
11 S. S. Duarte, D. K. F. Silva, T. M. H. Lisboa, R. G. Gouveia, R. C. Ferreira, R. O. de Moura, J. M. da Silva, E. D. A. Lima, S. Rodrigues-Mascarenhas and P. M. da Silva, *Anticancer Res.*, 2020, **40**, 5049–5057.
12 R. K. Bhaskarachar, V. G. Revanasiddappa, S. Hegde, J. P. Balakrishna and S. Y. Reddy, *Med. Chem. Res.*, 2015, **24**, 3516–3528.
13 P. Varakumar, K. Rajagopal, B. Aparna, K. Raman, G. Byran, C. M. Gonçalves Lima, S. Rashid, M. H. Nafady, T. B. Emran and S. Wybraniec, *Molecules*, 2022, **28**, 193.
14 M. Ramadan, Y. A. M. M. Elshaier, A. A. Aly, M. Abdel-Aziz, H. M. Fathy, A. B. Brown, J. R. Pridgen, K. N. Dalby and T. S. Kaoud, *Bioorg. Chem.*, 2021, **116**, 105344.
15 S. S. Duarte, D. K. F. Silva, T. M. H. Lisboa, R. G. Gouveia, C. C. N. de Andrade, V. M. de Sousa, R. C. Ferreira, R. O. de Moura, J. N. S. Gomes and P. M. da Silva, *Pharmacol. Rep.*, 2022, **74**, 545–554.
16 P. J. Patel, D. M. Patel, R. M. Vala, S. G. Patel, D. B. Upadhyay, Y. Pannerselvam and H. M. Patel, *ACS Omega*, 2022, **8**, 444–456.
17 I. R. Ager, A. C. Barnes, G. W. Danswan, P. W. Hairsine, D. P. Kay, P. D. Kennewell, S. S. Matharu, P. Miller and P. Robson, *J. Med. Chem.*, 1988, **31**, 1098–1115.
18 W. Raether, B. Enders, J. Hofmann, U. Schwannecke, H. Seidenath, H. Hänel and M. Uphoff, *Parasitol. Res.*, 1989, **75**, 619–626.
19 P. J. Patel, D. M. Patel, R. M. Vala, S. G. Patel, D. B. Upadhyay, Y. Pannerselvam and H. M. Patel, *ACS Omega*, 2023, **8**, 444–456.
20 R. M. Cross, J. R. Maignan, T. S. Mutka, L. Luong, J. Sargent, D. E. Kyle and R. Manetsch, *J. Med. Chem.*, 2011, **54**, 4399–4426.
21 N. Kausar, A. A. Masum, M. M. Islam and A. R. Das, *Mol. Diversity*, 2017, **21**, 325–337.
22 D. Song, X. Cao, J. Wang and S. Ke, *Bioorg. Med. Chem. Lett.*, 2020, **30**, 126826.
23 D. M. Patel, H. J. Patel, J. M. Padrón and H. M. Patel, *RSC Adv.*, 2020, **10**, 19600–19609.
24 D. B. Upadhyay, R. M. Vala, S. G. Patel, P. J. Patel, C. Chi and H. M. Patel, *J. Mol. Struct.*, 2023, **1273**, 134305.
25 S. G. Patel, P. J. Patel, D. B. Upadhyay, A. Puerta, A. Malik, N. K. Kandukuri, R. K. Sharma, J. M. Padrón and H. M. Patel, *J. Mol. Struct.*, 2023, **1292**, 136174.
26 D. M. Patel and H. M. Patel, *ACS Sustain. Chem. Eng.*, 2019, **7**, 18667–18676.
27 S. G. Patel, R. M. Vala, P. J. Patel, D. B. Upadhyay, V. Ramkumar, R. L. Gardas and H. M. Patel, *RSC Adv.*, 2022, **12**, 18806–18820.
28 S. G. Patel, A. González-Bakker, R. M. Vala, P. J. Patel, A. Puerta, A. Malik, R. K. Sharma, J. M. Padrón and H. M. Patel, *RSC Adv.*, 2022, **12**, 30404–30415.
29 P. J. Patel, R. M. Vala, S. G. Patel, D. B. Upadhyay, D. P. Rajani, F. Damiri, M. Berrada and H. M. Patel, *J. Mol. Struct.*, 2023, **1285**, 135467.
30 I. Tankov, R. Yankova, S. Genieva, M. Mitkova and D. Stratiev, *J. Mol. Struct.*, 2017, **1139**, 400–406.
31 J. M. Farber and P. I. Peterkin, *Microbiol. Rev.*, 1991, **55**, 476–511.
32 A. Daina and V. Zoete, *ChemMedChem*, 2016, **11**, 1117–1121.

33 M. J. Frisch, G. W. Trucks, H. B. Schlegel, G. E. Scuseria, M. A. Robb, J. R. Cheeseman, G. Scalmani, V. Barone, G. A. Petersson and H. Nakatsuji, *Gaussian 16*, Wallingford CT, 2016, vol. 421.
34 T. A. Keith and J. M. Millam, *gausview 6.1.1*, Semichem Inc., 2016.
35 O. Trott and A. J. Olson, *J. Comput. Chem.*, 2010, **31**, 455–461.
36 A. Daina, O. Michielin and V. Zoete, *Sci. Rep.*, 2017, **7**, 42717.